Dispersion and Effects of Metal Impregnated Granular Activated Carbon Particles on the Hydration of Antimicrobial Mortars

Ismael Justo-Reinoso[a], *Mark T. Hernandez*[a], *Catherine Lucero*[b] and *Wil V. Srubar III*[a,c,1]

[a] Department of Civil, Environmental, and Architectural Engineering, University of Colorado Boulder, ECOT 441 UCB 428, Boulder, CO 80309-0428, USA. [b] United States Department of Interior, Bureau of Reclamation (USBR), Denver Federal Center, 6th & Kipling, Bldg. 67, Denver, CO 80225, USA. [c] Materials Science and Engineering Program, University of Colorado Boulder, 4001 Discovery Drive, Boulder, CO 80303, USA.

Abstract

Granular activated carbon (GAC) particles impregnated with antimicrobial metals were incorporated into cementitious materials for the express purpose of inhibiting biogenic concrete corrosion. We report herein the influence of such metal-laden GAC particles on the hydration of cement mortars when substituted for fine aggregate, as well as the dispersion of metal in the cured matrix. Isothermal calorimetry was utilized to study the influence of GAC without and with copper and/or cobalt on select hydration characteristics of ordinary portland cement (OPC) mortars. When 1% of the fine aggregate mass was replaced with GAC particles of similar size, total evolved heat in all formulations was similar, regardless of GAC pretreatment. However, as the substitution approached 10% of the fine aggregate mass, metal-laden GAC formulations imparted delays in heat liberation and lowered heat fluxes. Results also substantiate that metal-laden GAC particles participate in the enhanced uptake of the calcium that is normally liberated during cement mixing and that the water delivered with GAC particles is not readily available during the first 142 h of curing. Electron microprobe analysis (EMPA) elucidated that copper and cobalt were homogenously distributed throughout the cement paste with metal-laden GAC, with these metals concentrations localized in a 50-100 μm region surrounding the GAC particles. Compressive strengths were not affected by the presence of metal-impregnated GAC in the concentration ranges tested and reported herein.

[1]Corresponding author at: 1111 Engineering Drive, ECOT 441 UCB 428, Boulder, CO 80309, USA. T+1 303 492 2621
e-mail address: wsrubar@colorado.edu

Keywords: Activated carbon; antimicrobial mortar; cement hydration; heavy metals; electron microprobe analysis; isothermal calorimetry.

1. Introduction

1.1 Antimicrobial Mortar

As a general class of materials, granular activated carbon (GAC) constitutes a wide range of amorphous carbon-based materials prepared in such a way that they exhibit exceptionally high specific surface areas (>500 m^2/g) [1]. Activated carbon particles, either in powder or granular form, have been included in cement formulations for different purposes [2-12]. One emerging application of activated carbon concerns metal-impregnated GAC particles that have been used to create a new class of antimicrobial cementitious materials that chemically inhibit microbially induced concrete corrosion (MICC) [9, 13].

Biogenic concrete corrosion is not a new phenomenon. The biological progression of microbial-induced corrosion in wastewater conveyance systems has been previously described and studied in depth, and comprehensive reviews on the topic are available [15-20]. Some sulfur-oxidizing microorganisms (SOMs) that colonize sewer infrastructure have demonstrated an inherent sensitivity to heavy metal exposure [21, 22]. Previous researchers have since incorporated metals, such as copper (Co), cobalt (Co), Zinc (Zn), and Nickel (Ni) into cementitious materials for the express purpose of conferring antimicrobial properties to wastewater conduits. Dry zeolites loaded with specific heavy metals, for example, have been used in different cement formulations to inhibit microbial corrosion [8, 23, 24].

Other carriers, including GAC, can impart antimicrobial resistances to solid materials. In this context Caicedo Ramirez and co-workers [13] showed that the growth of the most common SOM associated with corroding sewers, *Acidithiobacillus spp.*, could be inhibited by heavy metals loaded onto activated carbon according to the following hierarchy: Cu > Co > Cd > Zn = Ni. Additionally, when Co and Cu were simultaneously loaded onto activated carbon, the inhibition potential was seven times that of Co alone, while the Cu-inhibition potential remained unchanged.

While other literature also supports the premise that activated carbon can be used to carry antimicrobial metals in cement formulations [8, 9, 13], carbon-based particles have been traditionally considered a potential aggregate contaminant in cementitious materials [25-27]. More recent studies, however, have shown that substitutions of up to 2% of fine aggregate with GAC or powdered bituminous activated carbon can result in reproducible improvements to the hardened-state properties of ordinary portland cement (OPC) mortars [4, 12, 28, 29]. The use of engineered, biocidal metal-laden GAC particles in cementitious materials has since emerged as a promising new approach to inhibit the acidophilic microorganisms responsible for biogenic concrete corrosion [8, 9]. Recent research has been conducted with acid-treated GAC particles to understand the effects that the addition of these particles may have on the fresh- and hardened-state properties of antimicrobial OPC mortars [29].

Even though OPC pastes and mortars have been intensively studied for decades, cement hydration behavior remains an active research area [30, 31], especially in light of the myriad of emerging mineral and chemical admixtures that can affect the kinetics of cement hydration. Cement hydration involves a combination of dissolution and precipitation processes with complex interfacial interactions that may be influenced by the presence of heavy metals. The literature concerning the effects of heavy metals in this context remains limited and tenuous. However, there is emerging concurrence that heavy metals impart the most impact during the early stages of cement hydration [32-36]. Metals that are released into the pore solution of cementitious materials can react with, or otherwise sorb to, colloidal gel-like particles (*i.e.*, C-S-H) and/or form new compounds, including stable metal hydroxides [36, 37]. The early-age effects of different types of carbon-based materials (with no metals) on the kinetics of tricalcium silicate (C_3S) hydration have been reported by Sobolkina *et al.* (2016) [38]. In this work, mesoporous carbon (mean size of 13.9 μm) and HNO_3-treated carbon nanotubes (CNT) were found to have a catalytic effect on early C_3S hydration. There is a paucity of fundamental materials investigations reporting effects metal-laden carbon-based materials can have on the hydration of antimicrobial OPC pastes or mortars.

1.2 Scope

In response, the purpose of this study was to investigate the effects on cement hydration of mortars with increasing proportions of fine aggregate with two types of similarly sized bituminous GAC particles (HNO_3-treated and unmodified), including the effects of antimicrobial metal impregnation with copper and cobalt, alone and in combination. Up to a certain maximum, substituting GAC has been previously demonstrated [28] to confer compressive strength advantages over an otherwise identical formulation with no GAC, regardless of the presence of metal. Because curing behavior response to GAC has yet to be investigated, GAC effects on cement hydration were determined by evaluating temporal heat liberation patterns using accepted isothermal calorimetry methods adapted for mortar specimens [39-42]. Additionally, electron microprobe analysis (EMPA) was employed to map the concentrations and location of the antimicrobial metals throughout the mortar samples. The following formulations were analyzed: ten (10) formulations in which a pre-determined proportion of the fine aggregate was replaced by two different types of GAC particles—without and with metal impregnation—at an effective water to cement $(w/c)_{eff}$ ratio of 0.45; two (2) formulations where no fine aggregates were replaced by GAC, but where an amount of water equivalent to that carried by GAC was included in the initial mixing water; and, lastly, one (1) control formulation with no GAC substitution ($(w/c)_{eff}$ = 0.45). No other admixtures were used in this study. Metal-laden GAC substitution of 1% and 10% of the fine aggregate mass was chosen based on previous studies by the authors that have identified antimicrobial effectiveness in this range. Here, we report dose-dependent, time-series strength responses with heat liberation patterns for validation and completeness.

Materials and Methods

2.1 Materials

2.1.1 Ordinary Portland Cement (OPC)

A commercial OPC Type I/II manufactured by Quikrete (USA) that complies with ASTM C150-18 [43] was used in this study. The alkali- and metalloid-oxide content, along with a standard composition analysis (% by mass) of the cement, with its normative composition determined *via* Bogue analysis, has been previously presented in detail [28].

2.1.2 Granular Activated Carbon (GAC)

Granular activated carbon (GAC), manufactured from bituminous coal and commercially sold as OL 20x50, was supplied by Calgon Carbon Corporation (Pittsburgh, USA). GAC was used in two forms, namely (1) as-received (unmodified) and (2) after subjecting it to an acidification process with nitric acid (HNO_3-treated) as previously described elsewhere [29]. These two different types of GAC (i.e., unmodified and acidified) were considered in this study as they have been previously used in cementitious materials to purposely inhibit acidophilic growth in combination with sorbed heavy metals [8, 9, 13]. The purpose of using GAC after a specific acidification process was to enhance the chelation effect between the negatively charged surface of GAC and the metal cations (*i.e.*, copper) by increasing the number of acidic functional groups on its surface. Additionally, a specific point of zero charge (PH_{PZC}) for these particles was achieved (4.5-5) to favor leaching of the metals at pH levels relevant to the inhibition of targeted acidophilic microorganisms [9, 45]. These two types of activated carbons will be respectively referred to herein after as GAC-U (unmodified granular activated carbon) and GAC-A (acid-treated granular activated carbon with HNO_3). A complete characterization of the two GAC types used in this study (GAC-U and GAC-A), as well as a detailed acid-washing protocol, their Brunauer-Emmet-Teller (BET) surface areas, micro- and meso-pore volumes, pore size distributions, water saturation potentials, gradation analysis, and saturated surface dry (SSD) bulk specific gravity, is described in previous papers by the authors [28, 29].

2.1.2.1 Copper (Cu) and Cobalt (Co) sorption

To obtain metal-laden GAC, these particles were impregnated with soluble metals up to their saturation capacity according to the following scenarios: the GAC-U was loaded with two different metal

formulations (*i.e.*, Co or Co/Cu), while the GAC-A was loaded only with Cu. The sorption process was performed as follows. First, Cu $(NO_3)_2$ was added to a volume of deionized water needed to reach a 12mM Cu concentration and the pH adjusted (7.6-8) using NaOH to reach the optimum pH range to favor copper precipitation in hydroxide forms. Next, GAC-U was added to this solution in a liquid-to-solid ratio of 20:1 and mixed for 24 h at 150 r/min and room temperature. After 24 h, the pH of the solution was adjusted again to 7.6 and mixed at 150 r/min for another 24 h. After this process, the Cu-laden GAC (GAC-U-Cu) was separated from the solution, rinsed with water, and oven dried at 40 °C. A similar procedure was performed to create the GAC particles that included both Cu and Co; however, in addition to $Cu(NO_3)_2$, $Co(NO_3)_2$ was also dissolved in the initial solution (12 mM Co concentration) prior to GAC-U addition. Once the metals were completely dissolved, GAC-U was added and the process continued in a similar way as when only copper was originally dissolved. At the end, the Cu/Co-laden GAC-U (GAC-U-Cu/Co) was separated from the solution, rinsed with water, and oven dried at 40 °C.

Acidified GAC (GAC-A) was loaded with Cu by adding $Cu(NO_3)_2$ to a specific volume of deionized water to obtain a 12 mM Cu concentration, then the pH of this solution was raised using NaOH to the highest pH achievable where cationic Cu species were dominant in solution (5.6-6). Next, GAC-A was added to the solution in a liquid-to-solid ratio of 20:1 and mixed for 24 h at 150 r/min. After this time (24 h), the GAC-A was separated from the solution, and oven dried at 100 °C for 5 h and left to cool at 20 °C for 1 hr. Once the GAC-A was dry, a new solution was prepared as presented above, and the dry GAC-A was added to this new Cu solution and mixed for 24 h at 150 r/min. After this process, the Cu-laden GAC-A (GAC-A-Cu) was separated from the solution in a similar way as it was done for the GAC-U. Metals sorbed by these GAC particles were confirmed by Inductively Coupled Plasma Optical Emission Spectroscopy (ICP-OES) using a calibrated ARL 3410+ and modifications to a widely accepted technique developed by Farrell *et al.* [46]. Five mL of a mixture (7:3) containing hydrochloric acid and hydrofluoric acid were mixed with 2 mL of nitric acid and placed in plastic digestion tubes that were maintained at 95 °C in a digestion block (HotBlock, Environmental Express) for approximately two hours. Samples were

then cooled and brought to 50 mL with a solution of 1.5% boric acid (by mass). Samples were the reheated to 95 °C for 15 min and cooled for analysis. The samples were diluted 10x with deionized water and analyzed with an ICP-OES. Metal contents, which were normalized by the original GAC mass, are presented in **Table 1**.

Table 1: Concentration of Cu and Co sorbed onto the GAC particles surface. All GAC particles were loaded to their maximum sorption capacity.

GAC (type)	Copper (Cu) (mgCu/gGAC)	Cobalt (Co) (mgCo/gGAC)
GAC-U-Cu	13.0	0.0
GAC-U-Cu/Co	12.8	4.5
GAC-A-Cu	10.4	0.0

2.1.3 Graded Standard Sand (Ottawa Sand)

Ottawa sand was obtained from U.S. Silica Company (USA). Ottawa sand is a clean, natural sand with high silica content (99.0 – 99.9 % crystalline silica (quartz) [47]) that conforms to ASTM standard C778-17 [48]. Water saturation potential and SSD bulk specific gravity were determined in accordance with ASTM standard C128-15 [49] and presented in a previous paper by the authors [28].

2.2 Experimental Methods

2.2.1 Sample Formulations

The nomenclature of all sample formulations is summarized in **Table 2**. Cement mortars containing GAC (GAC-U or GAC-A) loaded with metals (Cu or Cu/Co) and reference cement mortars including the same GAC types without heavy-metal loading were prepared. All formulations, along with a control formulation containing no GAC particles, were prepared with a $(w/c)_{eff} = 0.45$ and a sand-to-cement ratio of 2.1. Additionally, two formulations were prepared without the addition of GAC, but these samples contained an identical amount of additional water as the water sorbed by GAC particles in an otherwise similar GAC-containing formulation. All samples are denoted according to the following scheme: type of

GAC used (U or A); type of metal(s) sorbed onto the GAC (Cu, Cu/Co or Ø (for no metal)), and, lastly, percentage of GAC substitution (1% or 10%). The formulations containing no GAC particles were labeled as follows: Control (for the reference formulation), EQUIV-1%GAC, and EQUIV-10%GAC, where the latter two formulations required an additional amount of water equivalent to the free water sorbed by GAC to be added to the mixing water. Three cement paste formulations containing GAC-U with Cu, GAC-U with Cu/Co, and GAC-A with Cu, respectively, were also included for elemental surface-mapping with an electron microprobe analysis (EMPA). The total amount of water used in these formulations included the water sorbed by the GAC plus the mixing water required to achieve a $(w/c)_{eff}$ = 0.45. Water internally sorbed by GAC is not immediately available for cement hydration. Therefore, moisture carried by GAC is not included with the conventional mixing water mass and not considered in the *w/c* ratio of the mix design. If GAC particles are saturated with water before being incorporated into the cement mortar formulations (as it was done in this study), they do not have an impact on the initial *w/c* ratio [50-52]. The total amount of water sorbed into GAC, in addition to that provided for initial mixing, is summarized in **Table 2** as $(w/c)_{add}$. This additional *w/c* ratio ($(w/c)_{add}$) contributes to the $(w/c)_{total}$. The effective *w/c* ratio ($(w/c)_{eff}$) takes into account the amount of water sorbed by the GAC particles. For the formulations with no GAC, but with the same amount of water as the ones containing GAC in 1% and 10% replacements, all water used is considered as mixing water, which results in an increase in the $(w/c)_{eff}$ of each formulation.

Table 2: Mortar formulations with their corresponding *w/c* ratios.

Formulation	$(w/c)_{add}$	$(w/c)_{total}$	$(w/c)_{eff}$
Control	0.00	0.45	0.45
U- Ø -1%	0.03	0.48	0.45
U-Cu-1%	0.03	0.48	0.45
U-Cu/Co-1%	0.03	0.48	0.45
A- Ø -1%	0.03	0.48	0.45
A-Cu-1%	0.03	0.48	0.45
U- Ø -10%	0.27	0.72	0.45
U-Cu-10%	0.27	0.72	0.45
U-Cu/Co-10%	0.27	0.72	0.45
A- Ø -10%	0.27	0.72	0.45

A-Cu-10%	0.27	0.72	0.45
EQUIV-1%GAC	0.00	0.48	0.48
EQUIV-10%GAC	0.00	0.72	0.72

2.2.2 Mixing Procedure

Prior to mixing, the GAC component was oven-dried at 90 °C for 24 h, air cooled, then submerged in water for 12 ± 1 h. The water used to saturate GAC prior to mortar formulation, was also factored into the bulk mixing water to maintain a 0.45 *w/c* ratio at formulation. All mortar formulations were manually mixed as follows. Firstly, cement was added to the total amount of water and GAC and mixed for 30 s. Then, the total amount of fine aggregate (Ottawa sand) was added and mixed for an additional 30 s. After these first 60 s, mortars were mixed for an additional 1 min for a total maximum mixing time of 2 min.

2.2.3 Isothermal Calorimetry

Heat flow (mW/g) was measured at the U.S. Bureau of Reclamation (USBR-Denver) using a TAM Air 8-Channel standard volume isothermal calorimeter (TA Instruments, USA). The calorimeter included an array of reacting and non-reacting (control) channels that were capable of eight simultaneous comparative measurements. In this study, isothermal conditions (23 ± 0.03 °C) were maintained in the calorimeter cells. The reference material samples (located in the non-reacting control channels) consisted of 5.5 g of siliceous sand. All observations were made and reported in duplicate. Freshly mixed cement mortar (5.5 g) was weighed into a 20 mL glass ampoule for each sample. The glass ampoule was sealed and placed into the calorimeter within 5 min after initial mixing, and the heat liberated was continuously monitored and recorded for approximately 142 h. External mixing was applied to ensure complete mixing. For this reason, the initial heat emission after the cement contacted with the mixing water was not measured. As recommended by other cement calorimetry investigations that include external mixing protocols, the integration of the heat flow accounted for the influence of external mixing energy [40, 53]. In the case of OPC, the first 30 min of hydration contributes less than 6 J/g to the cumulative heat release of the sample [53]. Integration of the heat flow was thus started 30 min after the initial contact of mixing water with

cement to enable time for temperature equilibration, as described above. The heat liberated during hydration and the cumulative heat flow were normalized to the cement mass of the respective samples.

2.2.3.1 Calorimetry Set Times

Initial and final set times were determined based on the first derivative of the heat flow curves according to an identical procedure implemented in Hu J. *et al.* (2014) [54]. The first derivative of heat flow curves (d(q)/d(t)) was obtained from the original heat flow curves. The initial set time was defined as the time at which the first derivative curve reaches a maximum, while the final set was defined as the time at which the first derivative equals zero after the initial set time [54].

2.2.4 Compressive Strength

The compressive strength of cement mortar specimens for each formulation was executed under uniaxial compression in accordance with ASTM standard C109-16a [55]. After 7, 28 and 240-days of continuous curing (temperature 23 ± 2°C; RH > 95%), the compressive strength of triplicate samples was determined. Pressure was applied to specimens in a calibrated compression press at a load-controlled rate of 1.32 kN/s using an Instron compression test machine.

2.2.5 GAC Calcium (Ca^{2+}) Affinity

The Ca^{2+} ion affinity of the GACs used in this study was assessed for their adsorptive capacity of Ca^{2+}ions under water quality conditions that mimic those typically found in the pore solution of cement paste. Following the methodology used by Sobolkina *et al.* [38], a series of batch sorption experiments were executed. A total amount of 2 g of GAC (GAC-U and GAC-A) were dispersed in 40 mL of a 0.10M NaOH solution (pH 12.8) at different initial Ca^{2+}concentrations (400 and 1320 mg/L), using $Ca(NO_3)_2$ as the Ca^{2+}source. The GAC particles were allowed to equilibrate for 24 h at a temperature of 21 °C, after which they were allowed to settle, filtered from the solution, and oven-dried overnight at 40 °C. Ca^{2+} sorbed onto the GAC particles was determined by ICP-OES on a calibrated ARL 3410+ using modifications to a technique developed by Farrell *et al.* [46].

2.2.6 Electron Microprobe Analysis (EMPA)

2.2.6.1 Sample Preparation

Three different cement pastes containing (1) GAC-U loaded with Cu, (2) GAC-U loaded with Cu/Co, and (3) GAC-A with Cu were cast in circular plastic molds of 15 mm diameter and 10 mm height. The samples were demolded after 24 h and cured in moist conditions for 30 days. After that time, each sample was dried in a desiccator for one week. Each sample was then polished using a 180 grit diamond grinding pad on an 8" Hillquist water-cooled grinder to expose a polished cement surface. The sample surface was then ground using moderate pressure with 240 and 320 grit diamond grinding pads. A Logitech LP-50 polisher with a radially grooved cast steel lapping plate spinning at 70 r/min was used for preparing each working face of the samples, using as an abrasive a mix of 15% silicon carbide (Alfa Aesar superfine 600 grit) and water. Each sample was then hand polished in serial steps using a Logitech PM5 polisher incorporating Buehler TriDent polishing pads and an Allied polycrystalline diamond suspension (*i.e.*, 6μm, 3μm, and 1μm). The plate speed varied between 50 and 70 r/min. The samples were front-loaded under pressure until any surficial damage from a previous step had been repaired, as judged by visual inspection. This process was repeated every three to eight min per step, and varied based on the overall sample hardness. Between each polishing step, the specimens were rinsed in cold, clean water with a Bransonic sonicator. Finally, the backside of the sample was ground using the 320 grit vertical grinding disc and a sample arm on a Hillquist Thin Section equipment until the tops and bottoms of the cylindrical samples were parallel. The polished face of the samples was protected during the final step. After this preparation, the samples were embedded in an epoxy disc of 25 mm diameter and 15 mm in height for EMPA analysis.

2.2.6.2 EMPA Elemental Composition Mapping

In order to estimate the distribution of selected elements on the samples surface, five wavelength dispersive spectrometry (WDS) element maps of Ca Kα, Co Kα, Cu Kα, Si Kα, and S Kα were acquired for three different cement paste formulations containing the following GAC substitutions: GAC-U with

Cu/Co, GAC-U Cu, and GAC-A Cu. The EMPA data acquisition was performed at the University of Colorado Boulder geology laboratory on a JEOL JXA-8230 electron microprobe outfitted with EDS and WDS attachments. All samples were carbon-coated (ca. 15 nm thin-film) using an Edwards Auto306 dual coater to ensure identical conductivity and analytical conditions with accepted standards. Backscattered Electron (BSE) images were also obtained using the JEOL JXA-8230. The EMPA system was set at 15 keV accelerating voltage, 40nA beam current, and 1 μm beam diameter. The WDS element maps were acquired using an accelerating voltage of 15 keV and a 100nA beam current. The electron beam was defocused between 5 μm and 6 μm in order to match the pixel size of the maps. A per-pixel dwell time of 10 msec was used. Prior to the acquisition, each spectrometer was calibrated on a series of Astimex standard reference materials. The standards were as follows: Ca: plagioclase; Co: Co-metal; Cu: chalcopyrite; Si: orthoclase; and S: anhydrite. The Ca Kα, S Kα, and Si Kα maps were obtained using spectrometers equipped with large-area pentaerythritol (PET) monochromaters. The Co Kα and Cu Kα maps were obtained using spectrometers equipped with large area lithium fluoride monochromaters. The energy dispersive x-ray spectra (EDS) were acquired at 15 keV accelerating voltage and accumulated over a 30-sec interval. Results, expressed as net counts, are semi-quantitative, since each pixel may represent a mixture of two or more mineral phases.

2.2.7 Scanning Electron Microscopy (SEM)

High-resolution scanning electron microscopy (SEM) (SEM SU3500 from Hitachi (Japan)) was used to study the presence of hydration products inside GAC particles. A magnification of 1600x, an anodic voltage of 5 kV, and a current filament intensity of 0.13 nA was used in this study.

3 Results

3.1 Isothermal Calorimetry

Figure 1 summarizes the rate of heat liberated from cement hydration and the cumulative heat obtained from the following mortar formulations: fine aggregate (Ottawa sand) substitution with 1% and 10% (by mass), including one of two types of GAC (GAC-U and GAC-A) in the presence and absence of metals

sorbed to their capacity (Cu or Cu/Co). For clarity, the heat flow results are presented for the first 30 h of curing, while the cumulative heat are presented for the whole observation period (~150 h).

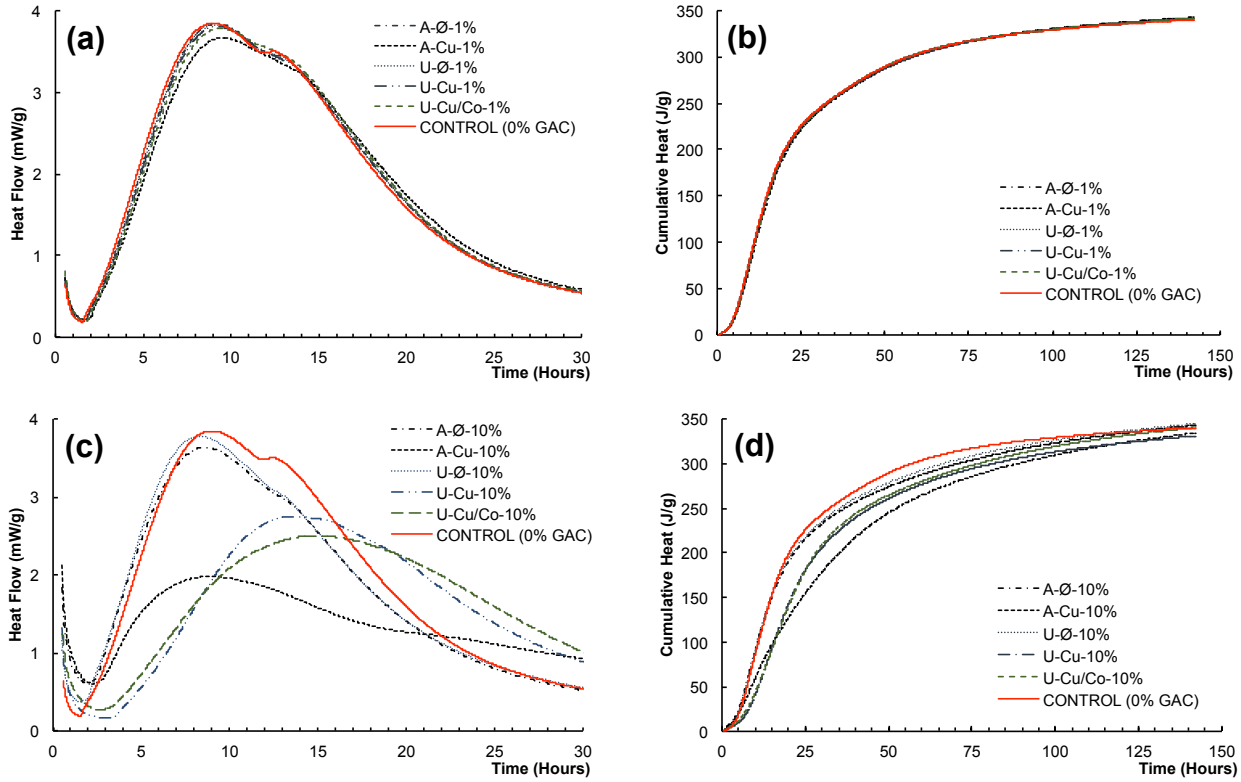

Figure 1: (a) Heat flow (mW/g) and **(b)** cumulative heat (J/g) for the following cement mortar formulations: Control (0% GAC), A-Ø-1%, A-Cu-1%, U-Ø-1%, U-Cu-1% and U-Cu/Co-1%; **(c)** Heat flow (mW/g) and **(d)** cumulative heat (J/g) for the following cement mortar formulations: Control (0% GAC), A-Ø-10%, A-Cu-10%, U-Ø-10%, U-Cu-10% and U-Cu/Co-10%. Each curve is representative of the mean of two measurements.

Following initial dormancy, an acceleration period, where the maximum heat release rate is observed, occurred between 1.6 and 1.9 h for all formulations with 1% sand substitution by GAC and the control; however, for the formulations including 10% sand replacement by GAC, initial acceleration was delayed between 1.9 and 3.5 h. The acceleration period was followed by a main heat rate peak between 9.2 and 9.6 h for the control and 1% GAC formulations, respectively, but between 8 and 15 h for the

different 10% GAC formulations. For all formulations with 1% sand replacement by GAC, regardless of the presence of metals, the sulfate depletion point is not clearly discernible as it is on the control formulation (0% GAC) (**Figure 1a**). Additionally, for the A-Cu-1% formulation, the height of the main peak (maximum heat rate peak) is slightly decreased, and a small delay in the heat rate curve could be observed as well. In **Figure 1b**, the cumulative heat for all the formulations containing 1% GAC substitutions and for the control (0% GAC) are presented. These results show that, regardless of the type of GAC employed or the presence or absence of metals, the cumulative heat flow plateaus at the same level (c.a. 341 J/g) at the end of the testing period (142 h).

In **Figure 1c**, the heat flow for the formulations containing 10% GAC replacements are compared to the control formulation (0% GAC). These results suggest that the increase in the amount of GAC replacement has a significant effect on the hydration of these formulations. For the formulations containing GAC that had not been impregnated with metals (*i.e.*, A-Ø-10% and U-Ø-10%) only a slight difference in heat emission patterns were observed during the 14 hours following mixing, where the A-Ø-10% formulation generated a slightly higher heat rate in the first 3 h than the latter (between 4 and 14 h), which was compensated by the U-Ø-10% formulation. When compared to the control formulation (0% GAC), the primary hydration peaks of these formulations were slightly accelerated and reduced in magnitude, and the peaks corresponding to calcium aluminate hydration were not easily distinguishable. On the other hand, when GAC particles impregnated with metals were incorporated into the mortar formulations, a slower heat release rate was observed for all formulations (*i.e.*, A-Cu-10%, U-Cu-10%, and U-Cu/Co-10%). The A-Cu-10% formulation, when compared to the other 10% GAC formulations containing metals, exhibited a higher heat emission rate during the first 9 hours of curing, after which the heat rate of the A-Cu-10% formulation began to decrease, resulting in the formulation with the lowest cumulative heat of all formulations tested. However, the cumulative heat after 142 h among all specimens with 10% of their fine aggregate substituted with GAC, regardless of the pre-treatment or presence of metals, ranged between 331 and 344 J/g **(Figure 1d)**. The two formulations with metal-laden GAC

particles that were not modified with nitric acid (*i.e.*, U-Cu-10% and U-Cu/Co-10%) behaved similarly with respect to its primary hydration peak when compared to the rest of the formulations with 10% fine aggregate replacement.

The cumulative heats for all formulations with 10% sand replacement by GAC are shown in **Figure 1d**. These data show that, when no metals were sorbed onto the GAC particles, the heat flow behavior is similar to the control formulation. On the other hand, the cumulative heat patterns were similar among the formulations with the metal-laden GAC-U particles (*i.e.*, U-Cu-10% and U-Cu/Co-10%). After 142 h, the two formulations with 10% sand replacement by GAC Cu-laden particles, independent of the type of GAC, reached the same cumulative heat, while the rest of the formulations (control, U-Cu/Co-10%, A-Ø-10%, and U-Ø-10%) exhibited a slightly higher cumulative heat.

The initial and final set times were obtained, and the results are shown in **Figure 2**. As mentioned by Hu *et al*. [54], due to the different mechanisms and test setups in determining setting times, longer setting times have been found from the calorimetry method when compared to ASTM penetration tests in similar cement mortar formulations. Nevertheless, the results obtained in this study, for the control and all formulations containing 1% GAC replacements, are congruent with the results obtained by Hu and coworkers for similar cement mortar formulations having no GAC additions [54]. The results indicated that the use of 1% GAC replacements, regardless the type or presence of metals, has no significant effect on the set times of these formulations, while, in contrast, the use of 10% GAC replacements, has a significant effect on the set times of these formulations. Formulations containing 10%, of either GAC-U or GAC-A with no metals, exhibited earlier set times when compared to all the formulations containing 1% GAC and the control, corroborating that the presence of GAC particles, regardless the type, has a catalytic effect on the hydration of C_3S, as it has been mentioned. An interesting finding is that regardless the presence of copper sorbed into the GAC surface, the formulation containing 10% Cu-laden GAC-A exhibited a similar behavior as the formulations containing 10% GAC with no metals, suggesting that the mechanism attaching the Cu to the GAC particle (*i.e.*, primarily through ionic interactions) is having an

effect on the way this Cu interacts with the hydration products that are formed during the first hours of the hydration process. On the other hand, the two formulations containing 10% GAC-U loaded with biocidal metals (*i.e.*, Cu or Cu/Co) presented a significant delay in their set times.

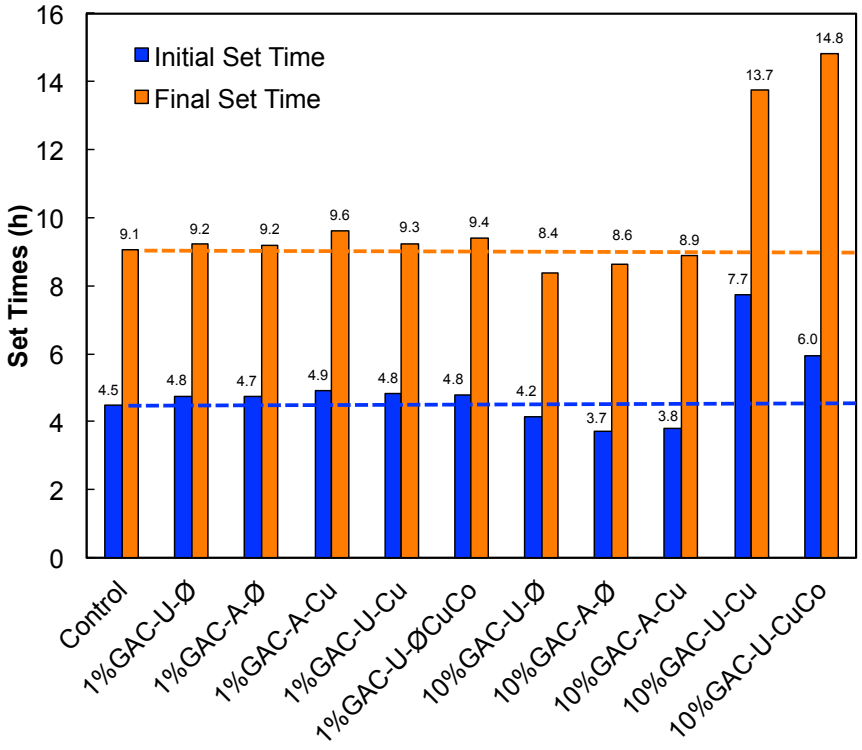

Figure 2: Initial and final set times calculated from the first derivative of the heat flow curves.

The heat flow and cumulative heat presented in **Figure 3a** and **3b** describe the behavior of formulations with no GAC as influenced by the different amounts of additional water that was absorbed by GAC for similar GAC replacements (1% and 10% GAC). The two shoulders evident in **Figure 3a** corresponding to the maximum heat and the accelerated calcium aluminate activity peaks are clearly visible. The cumulative heat of the sample with a *w/c* ratio equivalent to a 10% GAC replacement ($(w/c)_{eff}$ = 0.72), increased after approximately 14 h compared to the control formulation, while the formulation using a *w/c* ratio equivalent to a 1% GAC replacement ($(w/c)_{eff}$ = 0.48) behaved similarly to the control formulation ($(w/c)_{eff}$ = 0.45).

Figure 3c and **3d** presents comparisons of heat flow and cumulative heat from the following formulations: control, EQUIV-10%GAC with a $(w/c)_{eff} = 0.72$, and the respective 10% sand replacements—either by using GAC-U or GAC-A particles that did not carry metals. The EQUIV-10%GAC formulation presented a delay in its heat flow pattern when compared to the others; however, the EQUIV-10%GAC formulation presented no significant difference in its heat flow pattern, where the two distinguishable peaks exhibited by the control formulation (*i.e.*, in the main hydration peak) were clearly present in this formulation. The presence of these double peaks on the main hydration peak was not a clearly distinguishable thermodynamic pattern associated with formulations containing 10% sand replacement by GAC.

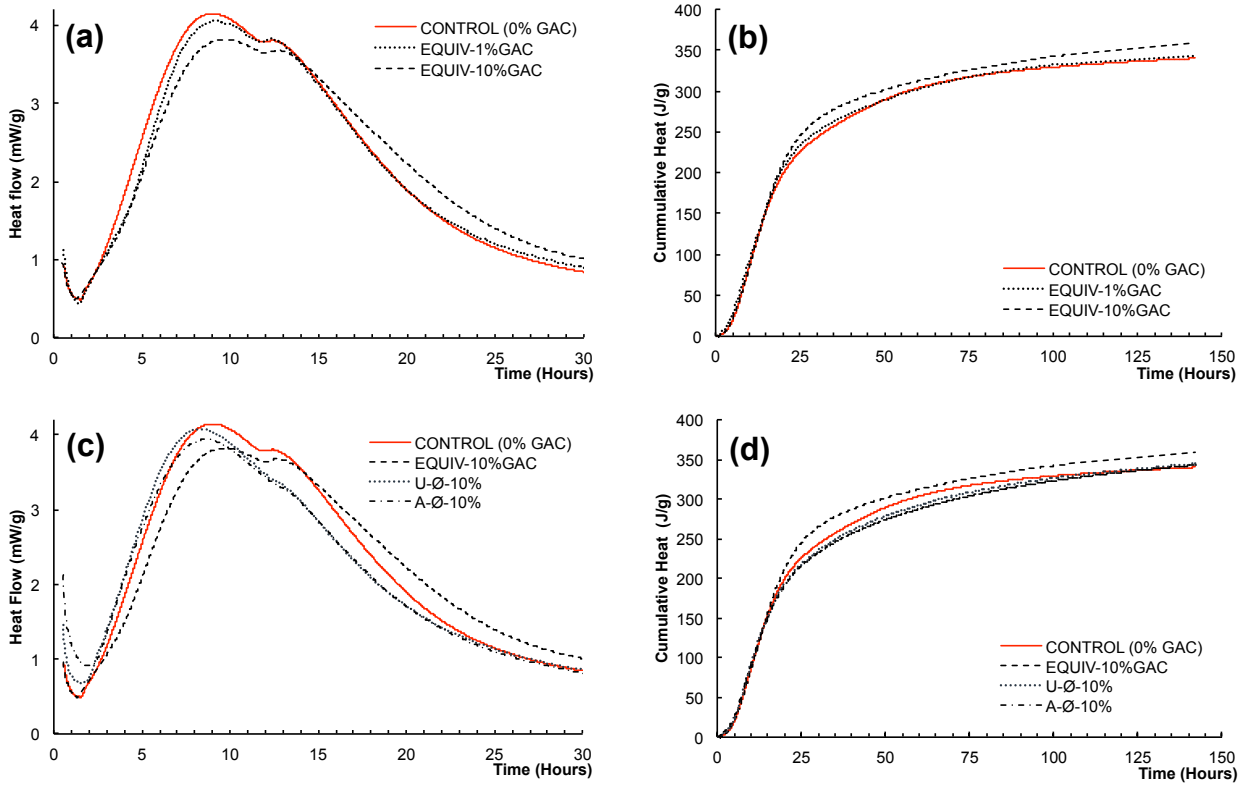

Figure 3: (a) hydration heat flow (mW/g) and **(b)** cumulative heat (J/g) for the following cement mortar formulations: Control (0% GAC), EQUIV-1%GAC and EQUIV-10%GAC; **(c)** hydration heat flow (mW/g) and **(d)** cumulative heat (J/g) for the comparison of the following cement mortar formulations:

Control (0%), EQUIV-10%GAC, U-Ø-10%, and A-Ø-10%. Each curve is representative of the mean of two measurements.

3.2 Compressive Strength

Results suggest that the substitution of 1% (by mass) of the fine aggregate with similarly sized GAC grains, regardless the presence or absence of biocidal metals, can manifest in an increase (up to 13.9 %) in the compressive strength of cement mortars (**Figure 4**). On the other hand, compressive strength decreased (up to 27.1%) with 10% GAC substitutions, regardless of the presence or absence of biocidal metals.

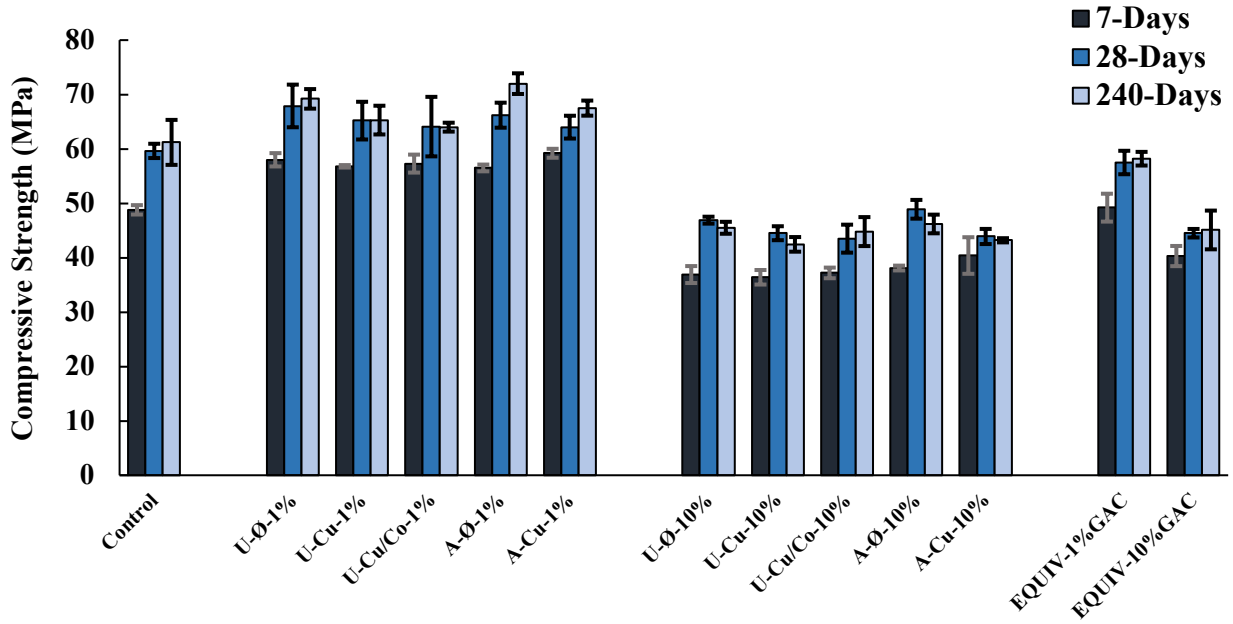

Figure 4: Average compressive strength of all formulations. Error bars represent ± one standard deviation.

The strength responses observed in this study are similar to results obtained in previous studies [28, 29] and demonstrate that GAC substitutions of 1% GAC (by mass) can systematically increase strength. It was also found that the presence of biocidal metals sorbed onto the GAC surfaces (either GAC-U or

GAC-A) did not have a significant effect on the compressive strength response of these mortar formulations (**Figure 4**). The conglomerate of strength responses observed herein could be attributed to the fact that the GAC used is acting as a pre-wetted lightweight aggregate and assisting with internal curing. However, derived from the heat flow curves, this assistance may not be significantly occurring during the first 142 h of the hydration process. Moreover, it is hypothesized that the shape of these GAC particles could have a positive effect on these strengths. It is known that rough angular particles could lead to improvements in strength of cementitious materials due to better interlocking between particles and the cement paste when compared with more rounded particles (*i.e.*, Ottawa sand) [57, 58]. In contrast, it was noted that, with 10% GAC substitutions, it appears that internal curing enhancements or the influence of the particle shape, cannot compensate for a concomitant decrease in the intrinsic compressive strength which results from replacing a silica grain with a weaker GAC particle [28].

3.3 Ca^{2+} Ion Affinity of GAC

Figure 5 summarizes batch tests mimicking the pore solution chemistry, where the sorptive interactions between pore solution Ca^{2+} and the GAC-U and GAC-A particles are isolated as the process variable. Hydrating cement mortars that include fine aggregate substitution by GAC particles have been hypothesized to sorb Ca^{2+} ions from pore solution [38]. This Ca^{2+} sorption potential is sensitive to the abundance of oxygen-containing functional groups on the GAC surface [38]. Under standard curing conditions, Ca^{2+} ions are released from OPC during cement hydration.

As is shown in **Figure 5**, increasing the Ca^{2+} ion concentration led to an increase in the amount of Ca^{2+} sorbed per unit mass of GAC particles. It is clear that the two types of GAC used here had significantly different sorption capacities for Ca^{2+} in simulated cement pore solution. Acid-treated GAC particles (GAC-A) had a higher Ca^{2+} sorption potential than their otherwise identical untreated counterparts (GAC-U) under the pore solution conditions tested herein.

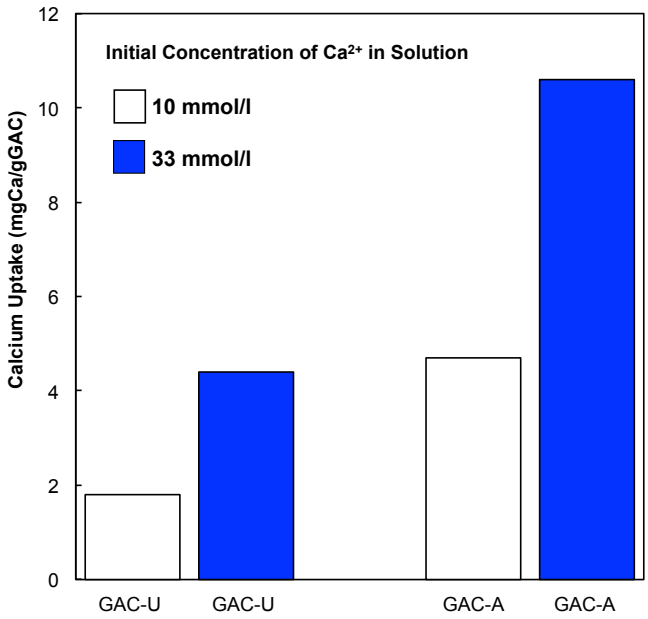

Figure 5: Evidence of sorption of Ca^{2+} ions by GAC particles from the pore solution.

3.4 Electron Microprobe Analysis (EMPA)

Wavelength dispersive spectroscopy (WDS) elemental mapping with energy dispersive x-rays spectroscopy (EDS) was used to assess the proximity of Cu and Co to the activated carbon particles, as well as the distribution of Ca, Si, and S throughout the cement matrix. WDS elemental maps of Cu and Co are shown in **Figure 6**. These BSE images show the location of the GAC particles as an overlayment on the elemental concentration maps of the respective metals. The EMPA maps substantiate that the location of Cu (and Co) is associated with the GAC particles and also revealed the existence of a concentration gradient near these particles within the cement matrix above the method detection limit (8 ppm). The highest metal concentrations were in the immediate proximity (50 to 100 μm region) surrounding the GAC particles, as expected. Microcracks present in the samples resulted during EMPA analysis, probably due to dessication and drying shrinkage that is likely to occur in the high vacuum conditions [40].

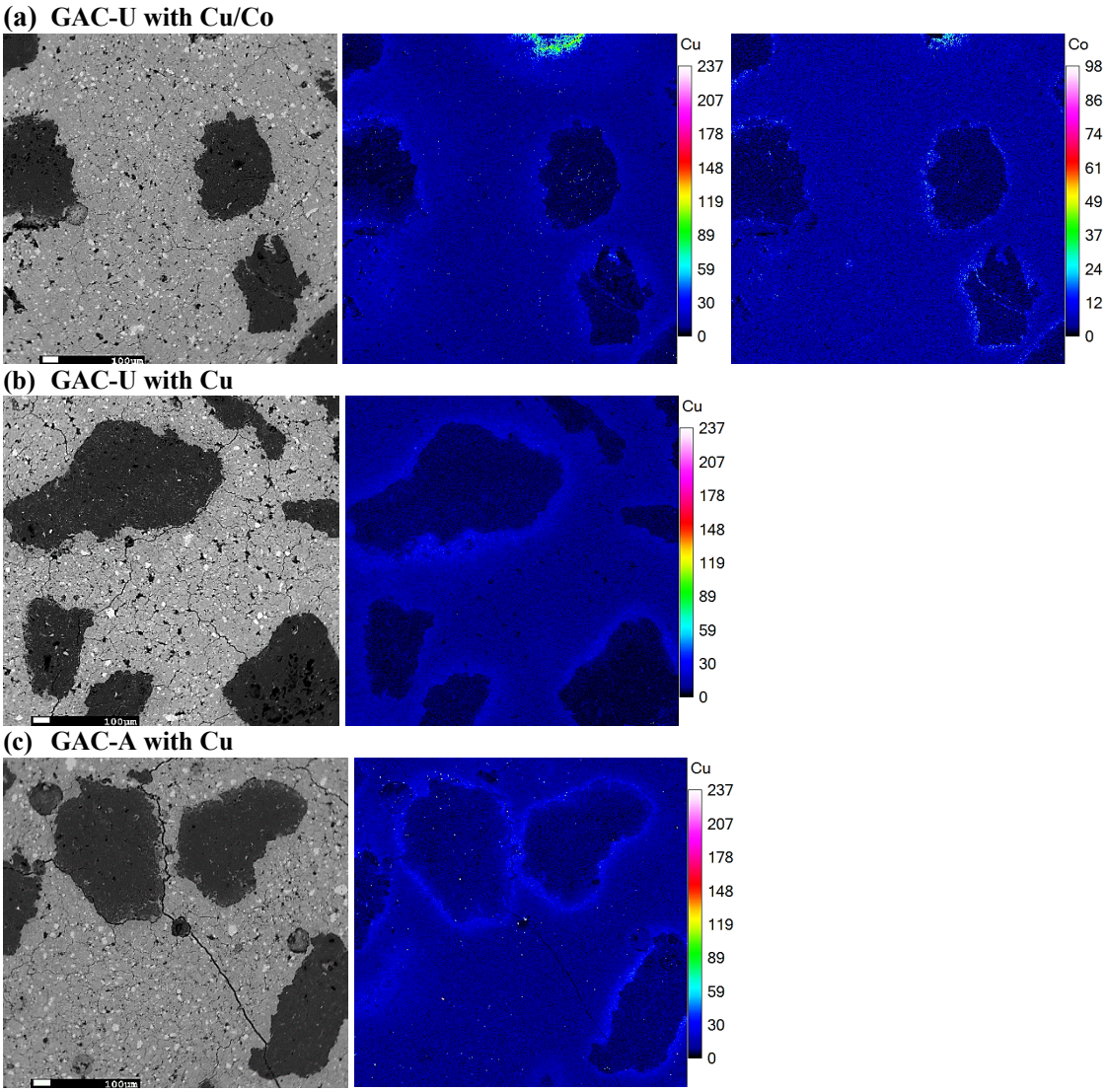

Figure 6: EMPA elemental maps of cement paste formulations after 30 days of standard curing. ***Left*** panels show BSE images of a given region; ***middle*** panels show Cu concentration distribution; and, in the ***right*** panel of **(a),** the GAC-U with Cu/Co formulation shows Co. The color scale on the right corresponds to relative integrated intensity obtained for each element. The intensity is proportional to the metal concentration.

WDS Ca elemental maps are presented in **Figure 7a**. The segmentation decomposition images focusing on the proximity of Ca to GAC particles is shown in **Figure 7b.** Ca levels are at their lowest

levels in and near the GAC particles, as evidenced by the radial pattern that extends between a 100 to 150 μm circumference around the GAC particles. On the other hand, S and Si concentrations were found to be uniformly distributed within the cement matrix with no significant changes in response to the proximity of GAC particles, regardless of metal loading (See Supplementary Information).

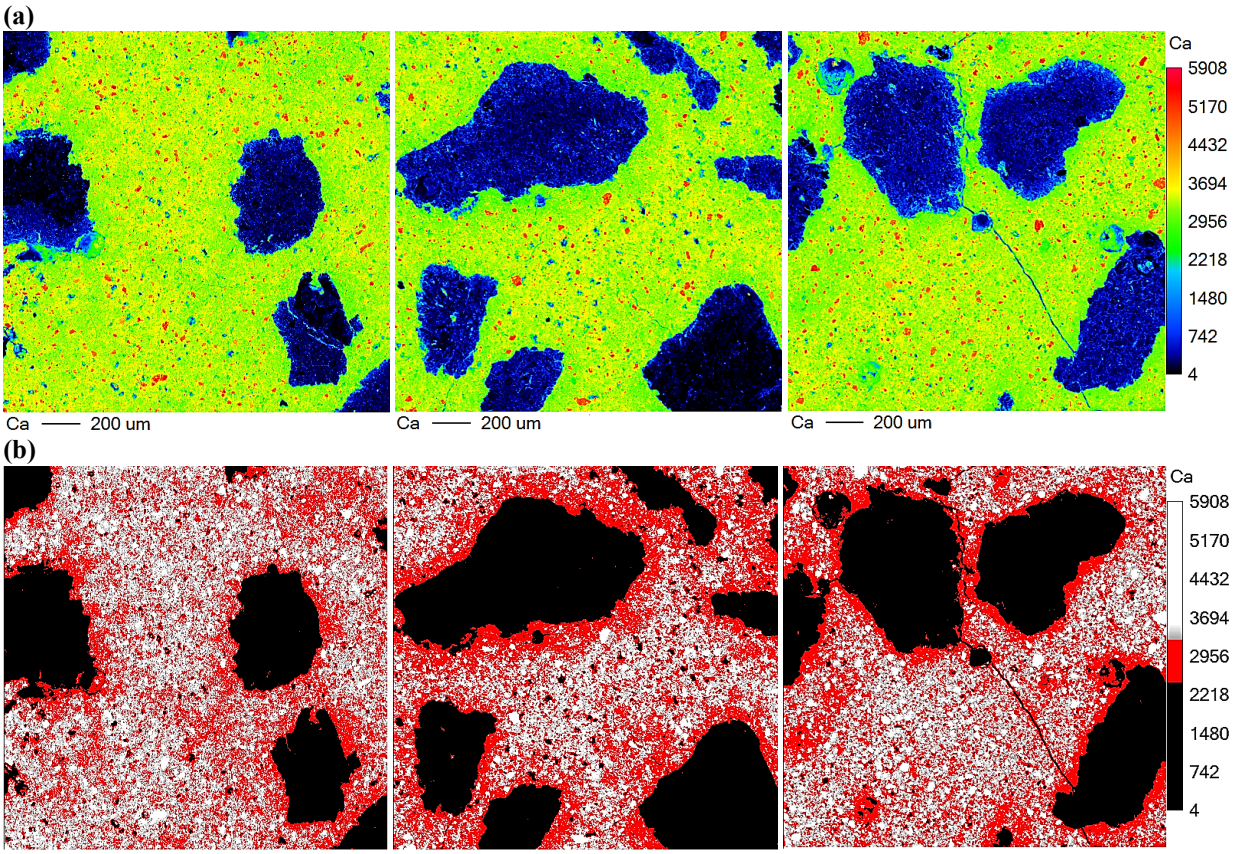

Figure 7: (a) WDS elemental mapping of calcium (Ca) after 30 days of curing: **(*left*)** GAC-U with Cu/Co, **(*middle*)** GAC-U with Cu, and **(*right*)** GAC-A with Cu; **(b)** Segmentation decomposition counts ranged between 2400 and 3200 relative to the Ca WDS elemental maps.

Five EDS spectra were obtained from formulations containing GAC-A-Cu and GAC-U-Cu. BSE images with the location points are shown in **Figure 8** and complete EDS spectra for these points of interest are shown in the Supplementary Information. Point **A** included mainly O, Ca, and Si and confirmed the

presence of an unhydrated cement grain, either a C_3S or C_2S particle. The elements identified at points B and D include carbon, oxygen, magnesium, aluminum, silicon, and calcium; while at points C and E, the main elements found were O, magnesium (Mg), aluminum (Al), Si, S, and Ca, suggesting the presence of C-S-H, portlandite, and ettringite. The peaks of carbon (C) were expected in all the EDS spectra, either as a result of the sample coating process with carbon or the carbonaceous composition of GAC particles.

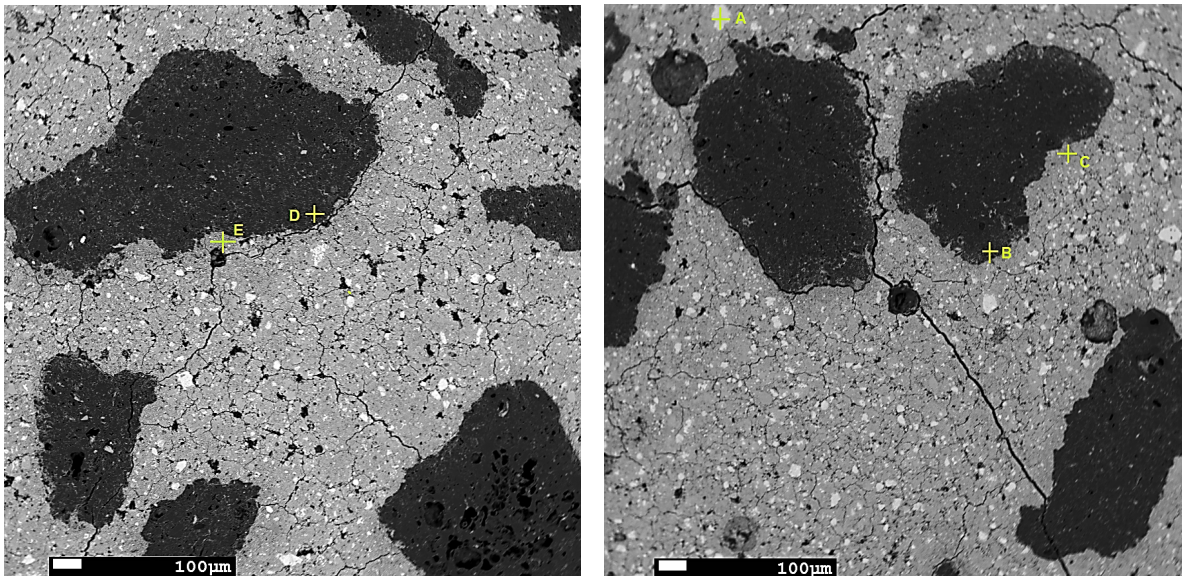

Figure 8: BSE images of cement pastes containing Cu-laden GAC-U ***(left)*** or Cu-laden GAC-A ***(right)*** are shown with the location points where energy dispersive x-ray spectra (EDS) were obtained. The EDS spectra corresponds to: **(a)** unhydrated cement; **(b)** copper laden GAC-A; **(c)** hydration products at interface of copper-laden GAC-A particle with cured cement matrix; **(d)** copper laden GAC-U particle; and, **(e)** hydration products at interface of copper laden GAC-U particle with cured cement matrix. Complete EDS spectra for these points of interest can be found in the Supplementary Information.

4 Discussion

4.1 Isothermal Calorimetry

4.1.1 Formulations Containing Metal-free GAC

The thermal power curve for the control formulation (0% GAC) shows a pattern typically associated with the hydration kinetics of OPC pastes and mortars [59]. Formulations with 1% sand replacement with metal-free GAC exhibited similar calorimetric behavior, regardless of acid pretreatment (**Figure 1a and 1b**). However, when comparing the two formulations containing 10% substitution of fine aggregate with metal-free GAC particles to the control formulation, the following effects were evident: (1) a not easily distinguishable sulfate depletion point; (2) an initial acceleration in the hydration rate of cement during the first 3 h; and (3) an earlier appearance of the primary hydration peak.

It is widely accepted that the sulfate depletion point may not be detectable in formulations containing different admixtures or certain supplementary cementitious materials (SCMs) or both [59]. Evidence for the physicochemical causes associated with the sulfate depletion conditions observed in this study included the following: 1) the primary C_3S hydration peak and accelerated calcium aluminate hydration peak (second peak) may be overlapping, implying that pore water sulfate is depleted earlier when GAC particles are included in an OPC formulation [60, 61]. Therefore, in the presence of GAC, the onset of the accelerated calcium aluminate activity would occur earlier. Several studies have demonstrated the sulfate sorption capacity of different activated carbons [62, 63], and this GAC sorption behavior could be associated with sequestering sulfate in the formulations containing GAC, as evidenced by the presence of sulfur in the EDS spectra of these GAC particles (see Supplementary Information).

Concerning formulations with a 10% substitution of GAC (no metals), calorimetry suggests that cement hydration is accelerated by the precence of GAC during the first 3 h of the hydration process. This initial hydration signature was higher for GAC-A when compared to the GAC-U and is likely associated with the increased presence of oxygen-containing surface functional groups on the acid-treated GAC-A particles. Several researchers [64-68] have characterized the functional group distributions when activated carbons are treated with HNO_3, and there is literature concurrence that strong acid treatment increases the number of acidic surface functionalities, resulting in a higher density of various oxygen-containing functional groups when compared to similar unmodified GAC surfaces. As suggested by Sobolkina and

coworkers [38], carbon-based materials with high specific surface areas and rich in oxygen-containing functional groups may have a catalytic effect on early C_3S hydration by both direct or indirect mechanisms. The direct mechanism proposed is mediated by the chemisorption of dissolved Ca^{2+} ions on carbon surfaces, which is consistent with the results summarized in **Figure 5**. Here, the acid-treated GAC-A particles clearly showed a higher Ca^{2+} uptake potential than their untreated GAC counterparts. It follows that a decrease in the concentration of dissolved Ca^{2+} ions at the initial hydration stage may cause an increase in the rate of C_3S dissolution. Furthermore, protons released into the aqueous phase by the acidic functional groups presented by GAC-A particles could decrease the local pH, which has the effect of promoting C_3S hydration [34, 38]. The indirect influence of acid-treated GAC, as suggested by Sobolkina *et al*. [38], may be associated with an increase in the C_3S surface area available for dissolution reactions as the result of the partial deposition of dissolved ionic products on the surfaces of GAC particles, where these particles act as seeds for the nucleation and growth of C-S-H. In contrast, untreated GAC particles show a lower affinity for Ca^{2+} ions as compared to their acid-treated counterparts, yet they exhibit higher adsorption of Ca^{2+} ions and an increased increment of nucleation sites when compared to the control formulation (not including GAC). The appearance of the maximum heat peak for the A-Ø-10% and U-Ø-10% formulations occurred earlier than their respective control formulation. This result could be explained by the promotion of earlier hydration reactions enhanced by the sorption and nucleation behavior suggested herein.

4.1.2 Formulations Containing Metal-laden GAC

Increasing the replacement of fine aggregate (sand) with 10% GAC particles (either GAC-U or GAC-A) loaded with Cu or Cu/Co, however, significantly modifies the hydration kinetics of cement mortars when compared to formulations that did not include GAC. It is well-known that the cement hydration process includes a complex combination of aqueous, dissolution/precipitation, and solid-state reactions that can be influenced by heavy metals—notably including Cu or Co [34, 36]. When any metal-laden GAC was present at a 10% mass substitution level, a significant delay in the early hydration process of all

formulations was observed. Several authors [33, 34, 61, 69] agree that the presence of metals may selectively delay cement hydration reactions due to a reduction of the permeability of cement grains; there is consensus that this curing rate reduction is likely caused by the rapid chemical precipitation of insoluble metal hydroxides on cement grains, which may reduce their permeability to water and other ions. This mechanism may be extended to the GAC surfaces when these particles are laden with Cu or Co. Weeks and coworkers [70] suggested that the curing retardation effect associated with heavy metals could also be induced by the conversion of a metal hydroxide to a metal hydroxyl-species, as this reaction consumes Ca^{2+} and hydroxide ions. This consumption would, in effect, delay the supersaturation of the cement pore water and, hence, the precipitation of C-S-H and portlandite.

A distinct secondary hydration peak associated with the calcium aluminate hydration at the sulfate depletion point was not evident in formulations with metal-laden GAC substitutions at a 10% substitution level (**Figure 1c**). This result is likely attributable to the partial sequestration of sulfates by GAC particles and/or Cu (as copper sulfate) from the pore solution during early-age hydration [61, 62]. It is important to mention that the formulations U-Cu-10% and U-Cu/Co-10% behaved very similarly during the first 80 hours of cement hydration. This finding can be explained by the fact that these two formulations included the same particle type (*i.e.*, GAC-U) and that the Cu, representing 100% and 74% of the total metal sorbed, respectively, is likely immobilized by surface precipitation as a metal hydroxide [71, 72]. However, in the corresponding formulations containing acid-treated GAC particles (A-Cu-10%), the attachment mechanism is thought to be primarily through ionic interactions with the oxidized functional groups introduced during the acidification process [68, 73]. As a result of having metals associating with GAC particles through markedly different mechanisms, the heat release rates observed were consistent with the pre-treatment of the substituted GAC particles (*i.e.*, acidified or unmodified) (**Figure 1c).** Comparing the cumulative heat released after 142 h of curing in **Figure 1d,** the presence of Cu, independent of the type of GAC used, clearly induces a delay in the hydration process. However, in the U-Cu/Co-10% formulation, the effect of Co loading with Cu manifests after 80 h, at which point there

is an acceleration of the hydration process when compared to the otherwise identical formulation containing only Cu (U-Cu-10%).

4.1.3 Formulations with w/c Ratios Equivalent to GAC Formulations

In the formulations where no fine aggregates were replaced by GAC, but where an amount of water equivalent to that carried by GAC for similar GAC replacements (1% and 10% GAC) was added, the calorimetry results obtained are in agreement with a generality in thermodynamic behavior for OPC formulations [39, 40, 56]. As the *w/c* ratio increased, the rates of heat liberation decreased, and the primary hydration peak was slightly delayed. This mechanism can be explained by shifts in pore water alkalinity and hydroxide concentrations, which is inversely dependent on the *w/c* ratio [40, 75].

Additionally, results from isolating GAC and *w/c* as process variables (**Figure 3d**), suggest that extra water sorbed into GAC particles is not readily available during the very early ages (*i.e.*, the first 142 h) of curing. However, after this period of time, additional water may be gradually available. Nevertheless, even if GAC particles in cement mortars may act as a distributed network of micro-reservoirs that sequester and deliver water in response to the progression of the curing process [28, 29], no conclusive evidence could be obtained in this study to show if the extra water associated with these GAC particles was available for otherwise enhanced hydration during the initial 142 h of the curing or if moisture egress from these particles was being blocked by localized nucleation of hydration products surrounding those GAC particles.

4.2 WDS Elemental Mapping

Regardless of GAC preparation, by far the highest metal levels remained at the interface of GAC particles and the bulk cement paste (**Figure 6**). However, it also is evident that some of the metals that were originally sorbed onto GAC particle surfaces experienced some degree of mobilization that resulted in their dispersement in low concentrations throught the matrix. While this metal diffusion away from the GAC particles was relatively small, these metals may be at a level and distribution which influences the

cement hydration process according to any or all of the mechanisms previously discussed. Furthermore, WDS elemental mapping from cement paste formulations containing metal-laden GAC particles (GAC-U and GAC-A), showed that in the areas immediately surrounding GAC particles, the concentration of calcium was consistently lower than in the rest of the bulk cement matrix (**Figure 7**). In contrast, silicon concentrations were equally distributed through the cement matrix, not observing areas with lower concentrations surrounding GAC particles (See **Figure S2** in the Supplementary Information). A possible explanation for this result may be the interactions between the hydration products and the biocidal metals present in higher concentrations at the interface of GAC particles and the bulk cement paste. As mentioned by Chen, Q. Y. *et al.*, (2007) [37], metals retard—and may temporarily inhibit—the precipitation of portlandite due to the reduction of pH (*i.e.*, < 12.4) resulting from the hydrolysis of heavy metal ions during C_3S hydration. This portlandite inhibition is even more pronounced in the presence of Cu that may have resulted in lower concentrations of Ca-related products. Additionally, during the early-age hydration, in C-S-H gel, metals may substitute for Ca, or metal hydroxides may substitute for portlandite. As a result, the Ca/Si ratio of these C-S-H gels is significantly decreased [37]. Another possible explanation, consistent with that of other authors [38], suggests that Ca^{2+} ions can be sequestered by carbon-containing particles in a way that effectively reduces the availability of free Ca^{2+} in their vicinity. Converging lines of evidence suggest that ions in the pore solution can interact with the GAC particles and form deposits of hydrated Ca-rich products, such as C-S-H, portlandite, and ettringite, in or on the GAC, as evidenced by the EDS results and SEM observations (**Figure 9**). A much more detailed analysis is necessary, however, for clarification of the interaction mechanisms between the metal-laden GAC particles and the development of hydration products around them.

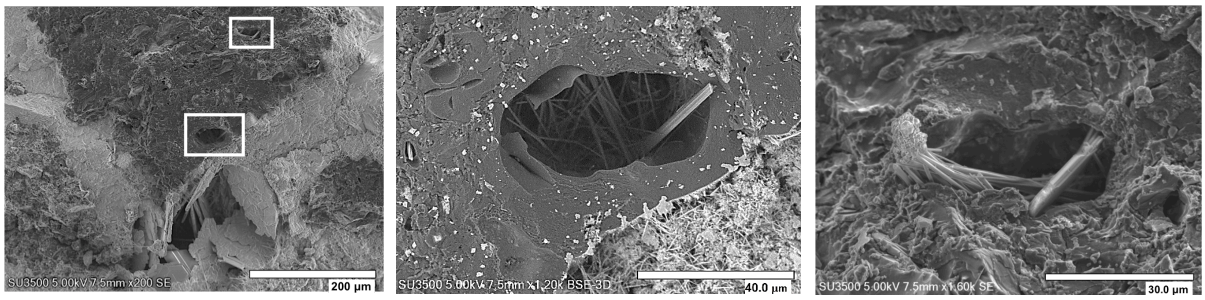

Figure 9: BSE images showing the surface of a GAC particle and morphologies of hydration products (ettringite) formed within the pores of the GAC particle.

5 Conclusions and Significant Findings

The antimicrobial effect of the use of metal-laden GAC particles in cement mortars to specifically inhibit microbially induced concrete corrosion (MICC) has been well documented before as an effective, potentially low-cost, long-term solution [8, 9, 13]. This study provides valuable insights on the use of these biocidal particles, with the aim to elucidate understanding of the effects that these antimicrobial aggregates have on the hydration process and mechanical properties of cement-based materials, and, in this way, expand mechanistic knowledge of materials designed to counter microbially-induced concrete corrosion.

The following statements highlight the conclusions and significant findings of this work:

- The use of 1% GAC replacements, regardless the presence or absence of biocidal metals, did not have significant effects on the hydration process of OPC mortars.
- The replacement of 10% fine aggregate with either GAC-U or GAC-A without associated metals accelerated the early hydration process and yielded a lower maximum heat rate when compared to otherwise identical control formulations.
- All the formulations containing 10% metal-laden GAC replacement exhibited lower maximum heat flows when compared to control formulation and other formulations that included 10% GAC substitutions. The formulations containing metal-laden GAC-U exhibited similar calorimetry

behavior, while the formulation containing metal-laden acid-treated GAC experienced the lowest maximum heat flow and significant delay in heat release.

- The use of higher replacement percentages (*i.e.*, 10%) of metal-lade acid-treated GAC particles did not have significant effects on the set times when compared to control formulations, contrary to what is observed when metal-laden unmodified GAC particles are used in similar replacement percentages.
- No significant difference was observed on the compressive strength behavior between formulations containing GAC-U or GAC-A, regardless of the presence or absence of biocidal metals, when these GAC particles were used as partial replacements (1% or 10% by mass) of fine aggregate in similar mortar formulations.
- Although at trace levels, Cu and Co were detectable throughout the cement matrix even though GAC was the only metal source, indicating that some metals desorbed from the GAC particles during cement hydration. However, metal is evident in relatively high concentrations in the immediate vicinity surrounding the GAC particles (50-100 μm). This implies the need for a correct spatial distribution of these GAC particles to obtain the desired antimicrobial effects.
- Depleted Ca levels were observed near the metal-laden GAC particles (100-150 μm). This depletion is hypothesized to occur in response to the isolated or combined effect of the following mechanisms: interactions between biocidal metals and hydration products, portlandite inhibition resulting from the reduction of pH derived from the hydrolysis of metal ions during the hydration period, metals substitution for calcium during C-S-H gel formation decreasing the Ca/Si ratio of the C-S-H, and/or sorption of Ca^{2+} ions by GAC particles.
- By isolating GAC and *w/c* as process variables, these results suggest that the extra water sorbed into GAC particles is not readily available during the first 142 h of cement hydration for the mortar formulations investigated herein.

6 Acknowledgments

The authors would like to thank the Bureau of Reclamation (USBR-Denver) for its help with conducting the calorimetry tests. Dr. Aaron Bell in the Department of Geological Sciences at the University of Colorado Boulder is also gratefully acknowledged for his assistance with EMPA. This research was supported by the Mexican National Council for Science and Technology (CONACYT) through Fellowship No.103259 and the Department of Civil, Environmental & Architectural Engineering at the University of Colorado Boulder through a Doctoral Dissertation Completion Fellowship. This work represents the views of the authors and not necessarily those of the sponsors.

REFERENCES

1. Çeçen, F. and Ö. Aktas, *Activated carbon for water and wastewater treatment: Integration of adsorption and biological treatment*. 2011: John Wiley & Sons.
2. Horgnies, M., I. Dubois-Brugger, and E.M. Gartner, *NOx de-pollution by hardened concrete and the influence of activated charcoal additions.* Cement and Concrete Research, 2012. **42**(10): p. 1348-1355.
3. Krou, N., et al., *Mechanisms of NO x entrapment into hydrated cement paste containing activated carbon—Influences of the temperature and carbonation.* Cement and Concrete Research, 2013. **53**: p. 51-58.
4. Erşan, Y.Ç., et al., *Screening of bacteria and concrete compatible protection materials.* Construction and Building Materials, 2015. **88**: p. 196-203.
5. Resheidat, M. and N. Al-Araji, *Effect of charcoal on the porosity and the properties of concrete*.
6. Elkouz, M.E., *Investigating the Physical Properties and Runoff Treatment Capability of Pervious Concrete Containing Granular Activated Carbon.* 2014.
7. Youn, J.-N., C.-Y. Sung, and Y.-I. Kim, *Physical and mechanical properties of porous concrete using waste activated carbon.* Journal of the Korean Society of Agricultural Engineers, 2009. **51**(4): p. 21-27.
8. Ling, A.L., *Characterization and Control of Microbially Induced Concrete Corrosion*, in *Civil, Environmental and Architectural Engineering*. 2013, Colorado University at Boulder: Boulder, CO.
9. Caicedo-Ramirez, A., *Doctoral Thesis: Antimicrobial Aggregates for the In-Situ Control of Microbially Induced Concrete Corrosion*, in *Department of Civil, Environmental, and Architectural Engineering*. 2018, PhD Thesis University of Colorado-Boulder: Boulder, Colorado (USA).
10. Krou, N., et al., *Reactivity of volatile organic compounds with hydrated cement paste containing activated carbon.* Building and Environment, 2015. **87**: p. 102-107.
11. Justo-Reinoso, I.A., *Microstructural Responses of Cementitious Materials to Substitutions with Fine Antimicrobial Aggregates*, in *Department of Civil, Environmental, and Architectural Engineering*. 2020, PhD Thesis University of Colorado-Boulder: Boulder CO USA. p. 248.
12. Lekkam, M., et al., *Influence of saturated activated carbon on the rheological and mechanical properties of cementitious materials.* Construction and Building Materials, 2019. **198**: p. 411-422.

13. Caicedo-Ramirez, A., A.L. Ling, and M. Hernandez, *Diffusion susceptibility demonstrates relative inhibition potential of sorbent-immobilized heavy metals against sulfur oxidizing acidophiles.* Journal of microbiological methods, 2016. **131**: p. 42-44.
14. Olmstead, W. and H. Hamlin, *Converting portions of the Los Angeles outfall sewer into a septic tank.* Engineering news, 1900. **44**(19): p. 317-318.
15. Grengg, C., et al., *Advances in concrete materials for sewer systems affected by microbial induced concrete corrosion: A review.* Water research, 2018. **134**: p. 341-352.
16. Buvignier, A., et al., *Resistance to biodeterioration of aluminium-rich binders in sewer network environment: Study of the possible bacteriostatic effect and role of phase reactivity.* Cement and Concrete Research, 2019. **123**: p. 105785.
17. Lors, C., E.D.H. Miokono, and D. Damidot, *Interactions between Halothiobacillus neapolitanus and mortars: Comparison of the biodeterioration between Portland cement and calcium aluminate cement.* International Biodeterioration & Biodegradation, 2017. **121**: p. 19-25.
18. Kaushal, V., M. Najafi, and J. Love, *Qualitative Investigation of Microbially Induced Corrosion of Concrete in Sanitary Sewer Pipe and Manholes*. 2018, Pipeline.
19. Wu, L., C. Hu, and W.V. Liu, *The Sustainability of Concrete in Sewer Tunnel—A Narrative Review of Acid Corrosion in the City of Edmonton, Canada.* Sustainability, 2018. **10**(2): p. 517.
20. Wells, T. and R. Melchers, *Modelling concrete deterioration in sewers using theory and field observations.* Cement and Concrete Research, 2015. **77**: p. 82-96.
21. De Muynck, W., N. De Belie, and W. Verstraete, *Effectiveness of admixtures, surface treatments and antimicrobial compounds against biogenic sulfuric acid corrosion of concrete.* Cement and Concrete Composites, 2009. **31**(3): p. 163-170.
22. Haile, T., et al., *Evaluation of the bactericidal characteristics of nano-copper oxide or functionalized zeolite coating for bio-corrosion control in concrete sewer pipes.* Corrosion Science, 2010. **52**(1): p. 45-53.
23. Haile, T. and G. Nakhla, *The inhibitory effect of antimicrobial zeolite on the biofilm of Acidithiobacillus thiooxidans.* Biodegradation, 2010. **21**(1): p. 123.
24. Haile, T. and G. Nakhla, *A novel zeolite coating for protection of concrete sewers from biological sulfuric acid attack.* Geomicrobiology Journal, 2008. **25**(6): p. 322-331.
25. ASTM, *C33/C33M-13 Standard Specification for Concrete Aggregates*. 2013, ASTM: West Conshohocken, PA, 19428, United States. p. 11.
26. ONNCCE, *NMX-C-111-ONNCCE-2014: Building industry- Aggregates for hydraulic concrete-Specifications and test methods.*, in *National Agency for Standardization and Certification of Building and Construction, S.C.* 2014, ONNCCE: Mexico D.F. p. 12.
27. Lamond, J.F. and J.H. Pielert. *Significance of tests and properties of concrete and concrete-making materials*. 2006. Astm West Conshohocken, PA.
28. Justo-Reinoso, I., et al., *Fine aggregate substitution by granular activated carbon can improve physical and mechanical properties of cement mortars.* Construction and Building Materials, 2018. **164**: p. 750-759.
29. Justo-Reinoso, I., et al., *Fine aggregate substitution with acidified granular activated carbon influences fresh-state and mechanical properties of ordinary Portland cement mortars.* Construction and Building Materials, 2019. **207**: p. 59-69.
30. Jansen, D., et al., *The early hydration of Ordinary Portland Cement (OPC): An approach comparing measured heat flow with calculated heat flow from QXRD.* Cement and Concrete Research, 2012. **42**(1): p. 134-138.
31. Zongjin, L., *Advanced concrete technology.* Hoboken, New Jersey: John Wiley & Sons, Inc, 2011.
32. Li, X., et al., *Heavy metal speciation and leaching behaviors in cement based solidified/stabilized waste materials.* Journal of Hazardous Materials, 2001. **82**(3): p. 215-230.

33. Tashiro, C. and J. Oba, *The effects of Cr2O3, Cu (OH) 2, ZnO and PbO on the compressive strength and the hydrates of the hardened C3A paste.* Cement and Concrete Research, 1979. **9**(2): p. 253-258.
34. Chen, Q., et al., *Immobilisation of heavy metal in cement-based solidification/stabilization: a review.* Waste management, 2009. **29**(1): p. 390-403.
35. Wiesława, N.-W., T. Barbara, and D. Sylwia, *The properties of cement pastes and mortars processed with some heavy metal nitrates containing solutions.* Procedia Engineering, 2015. **108**: p. 72-79.
36. Gineys, N., G. Aouad, and D. Damidot, *Managing trace elements in Portland cement – Part I: Interactions between cement paste and heavy metals added during mixing as soluble salts.* Cement and Concrete Composites, 2010. **32**(8): p. 563-570.
37. Chen, Q., et al., *Characterisation of products of tricalcium silicate hydration in the presence of heavy metals.* Journal of Hazardous Materials, 2007. **147**(3): p. 817-825.
38. Sobolkina, A., et al., *Effect of Carbon-Based Materials on the Early Hydration of Tricalcium Silicate.* Journal of the American Ceramic Society, 2016. **99**(6): p. 2181-2196.
39. Lura, P., F. Winnefeld, and S. Klemm, *Simultaneous measurements of heat of hydration and chemical shrinkage on hardening cement pastes.* Journal of thermal analysis and calorimetry, 2010. **101**(3): p. 925-932.
40. Scrivener, K., R. Snellings, and B. Lothenbach, *A Practical Guide to Microstructural Analysis of Cementitious Materials*. 2016, FL (USA): CRC Press. 540.
41. Wadsö, L., *Isothermal calorimetry for the study of cement hydration*. 2002: Division of Building Materials, Lund University.
42. Wadsö, L., *Applications of an eight-channel isothermal conduction calorimeter for cement hydration studies.* Cement international, 2005(5): p. 94-101.
43. ASTM, *C150/C150M-18 Standard Specification for Portland Cement*. 2018, ASTM: West Conshohocken, PA, 19428, United States. p. 10.
44. CalgonCarbon, *Granular Activated Carbon OL 20x50 Data Sheet*. 2015: Pittsburg, PA, USA.
45. Justo-Reinoso, I., et al., *Acidified granular activated carbon improves the rheological properties of ordinary portland cement mortars.* Construction and Building Materials (in review), 2018.
46. Farrell, R.F., S.A. Matthes, and A.J. Mackie, *Simple, low-cost method for the dissolution of metal and mineral samples in plastic pressure vessels*. 1980, Bureau of Mines, Washington, DC (USA).
47. Company, U.S.S., *Ottawa Sand Material Data Sheet*. 2012, U.S. Silica Company Frederick, MD 21701 USA. p. 12.
48. ASTM, *C778-17 Standard Specification for Standard Sand*. 2017, ASTM: West Conshohocken, PA, 19428, United States. p. 3.
49. ASTM, *C128-15 Standard Test Method for Relative Density (Specific Gravity) and Absorption of Fine Aggregate*. 2015, ASTM: West Conshohocken, PA, 19428, United States. p. 6.
50. (ACI), A.C.I., *ACI 213R-03 Guide for Structural Lightweight-Aggregate Concrete*, in *ACI Committee 213*. 2003. p. 38.
51. Sancak, E., Y.D. Sari, and O. Simsek, *Effects of elevated temperature on compressive strength and weight loss of the light-weight concrete with silica fume and superplasticizer.* Cement and Concrete Composites, 2008. **30**(8): p. 715-721.
52. Kosmatka, S.H., W.C. Panarese, and B. Kerkhoff, *Design and control of concrete mixtures*. Vol. 5420. 2002: Portland Cement Association Skokie, IL.
53. Justs, J., et al., *Influence of superabsorbent polymers on hydration of cement pastes with low water-to-binder ratio.* Journal of Thermal Analysis and Calorimetry, 2014. **115**(1): p. 425-432.

54. Hu, J., Z. Ge, and K. Wang, *Influence of cement fineness and water-to-cement ratio on mortar early-age heat of hydration and set times.* Construction and building materials, 2014. **50**: p. 657-663.
55. ASTM, *C109/C109M-16a Standard Test Method for Compressive Strength of Hydraulic Cement Mortars (Using 2-in. or [50-mm] Cube Specimens)*. 2016, ASTM: West Conshohocken, PA, 19428, United States.
56. Ge, Z., et al., *Characterization and performance prediction of cement-based materials using a simple isothermal calorimeter.* Journal of Advanced Concrete Technology, 2009. **7**(3): p. 355-366.
57. Donza, H., O. Cabrera, and E. Irassar, *High-strength concrete with different fine aggregate.* Cement and Concrete Research, 2002. **32**(11): p. 1755-1761.
58. Cortes, D., et al., *Rheological and mechanical properties of mortars prepared with natural and manufactured sands.* Cement and Concrete Research, 2008. **38**(10): p. 1142-1147.
59. ASTM, *C1679-17: Standard Practice for Measuring Hydration Kinetics of Hydraulic Cementitious Mixtures Using Isothermal Calorimetry*. 2017, ASTM: West Conshohocken, PA, 19428, United States. p. 15.
60. Zingg, A., et al., *Interaction of polycarboxylate-based superplasticizers with cements containing different C3A amounts.* Cement and Concrete Composites, 2009. **31**(3): p. 153-162.
61. Thomas, N., D.A. Jameson, and D. Double, *The effect of lead nitrate on the early hydration of Portland cement.* Cement and Concrete Research, 1981. **11**(1): p. 143-153.
62. Salman, M.S., *Removal of sulfate from waste water by activated carbon.* Al-Khwarizmi Engineering Journal, 2018. **5**(3): p. 72-79.
63. Hong, S., et al., *Adsorptive removal of sulfate from acid mine drainage by polypyrrole modified activated carbons: Effects of polypyrrole deposition protocols and activated carbon source.* Chemosphere, 2017. **184**: p. 429-437.
64. Chen, J.P. and S. Wu, *Acid/base-treated activated carbons: characterization of functional groups and metal adsorptive properties.* Langmuir, 2004. **20**(6): p. 2233-2242.
65. Gomez-Serrano, V., et al., *Mass and surface changes of activated carbon treated with nitric acid. Thermal behavior of the samples.* Thermochimica acta, 1997. **291**(1-2): p. 109-115.
66. Noh, J.S. and J.A. Schwarz, *Effect of HNO3 treatment on the surface acidity of activated carbons.* Carbon, 1990. **28**(5): p. 675-682.
67. Otake, Y. and R.G. Jenkins, *Characterization of oxygen-containing surface complexes created on a microporous carbon by air and nitric acid treatment.* Carbon, 1993. **31**(1): p. 109-121.
68. Moreno-Castilla, C., et al., *Activated carbon surface modifications by nitric acid, hydrogen peroxide, and ammonium peroxydisulfate treatments.* Langmuir, 1995. **11**(11): p. 4386-4392.
69. Mangabhai, R., *Calcium Aluminate Cements: Proceedings of a Symposium dedicated to HG Midgley, London, July 1990*. 2014: CRC Press.
70. Weeks, C., R.J. Hand, and J.H. Sharp, *Retardation of cement hydration caused by heavy metals present in ISF slag used as aggregate.* Cement and concrete composites, 2008. **30**(10): p. 970-978.
71. Romero, L.C., A. Bonomo, and E.E. Gonzo, *Peanut shell activated carbon: Adsorption capacities for copper (II), zinc (II), nickel (II) and chromium (VI) ions from aqueous solutions.* Adsorption Science & Technology, 2004. **22**(3): p. 237-243.
72. Inyang, M., et al., *Removal of heavy metals from aqueous solution by biochars derived from anaerobically digested biomass.* Bioresource technology, 2012. **110**: p. 50-56.
73. Yin, C.Y., M.K. Aroua, and W.M.A.W. Daud, *Review of modifications of activated carbon for enhancing contaminant uptakes from aqueous solutions.* Separation and Purification Technology, 2007. **52**(3): p. 403-415.

74. Golias, M., J. Castro, and J. Weiss, *The influence of the initial moisture content of lightweight aggregate on internal curing.* Construction and Building Materials, 2012. **35**: p. 52-62.
75. Danielson, U. *Heat of hydration of cement as affected by water-cement ratio*. in *Proc. 4th Int. Symp. on the Chem. of Cem., Washington, 1962*. 1962.